scientific reports

Check for updates

OPEN

Comparison of mediating effects of air pollutants on urban morphology and urban heat Island intensity at block scale

Jiayu Fan[1], Xuegang Chen[1]✉, Weihong Zhang[2], Mei Zhao[1] & Xinlu Yang[3]

The urban heat island effect seriously challenges the sustainability and livability of urban development. Air pollutants (AP) may play a mediating role in the impact of urban morphology (UM) on the canopy layer urban heat island intensity (CLUHII) and the surface urban heat island intensity (SUHII). To verify this hypothesis, taking Urumqi as an example, we use the ridge regression model to reveal the differences in the impacts of UM and AP on the two types of urban heat island intensity (UHII). A structural equation model was established to verify the mediating effect of AP. The results show that: (1) There are differences in the optimal research units for UM and CLUHII and SUHII, which are 500 m and 300 m respectively. (2) Whether it is CLUHII or SUHII, the impact of two - dimensional urban morphology indicators are greater than that of three - dimensional urban morphology indicators. (3) There are similarities and differences in the impact of urban morphology indicators on the two types of UHII. The effects of standard deviation of building height, floor area ratio, and sky view factor on the two are opposite. (4) Air pollutants (PM_{10}, $PM_{2.5}$, NO_2) have significant mediating effects between building density, impervious surface percent, green coverage ratio, mean building height, standard deviation of building height, floor area ratio, sky view factor, and the two types of UHII. This study provides a reliable reference for urban planning aimed at mitigating the urban heat island effect and air pollution.

Keywords Urban morphology, Urban heat Island intensity, Air pollutants, Mediating effects, China

Urbanization has propelled the continuous growth of urban land use area and urban building density, and the urban natural environment has undergone rapid changes[1]. In terms of urban land use, a large amount of natural vegetation and water bodies have been converted into construction land. The heat emitted by concrete and asphalt roads, the low ventilation capacity of urban canyons formed by high - rise buildings, and the combined effects of heat released by vehicles on the streets and air conditioners have led to changes in the urban climate[2,3]. The concentrated emissions from activities such as transportation and industry brought about by urbanization have exacerbated the air pollution problem[4]. These climate and environmental issues have increased the frequency of heatwaves and other extreme weather events, affecting the quality of the urban living environment as well as residents' health and safety[5–7]. To address the challenges associated with the evolving urban heat island effect, air pollution, and other related issues, scientific and reasonable urban planning and governance have become urgent tasks for planners in regulating the thermal environment and air pollution[8].

In recent years, the urban heat island (UHI) effect and its impacts on public health have emerged as critical challenges in the global urbanization process. Recent studies have focused on innovative multi-scale thermal environment regulation strategies and evaluation systems, revealing the effectiveness of multi-dimensional intervention pathways such as optimized vegetation layout, urban morphology control, and climate-adaptive planning. A study in Dalian demonstrated that canopy planning in urban plazas reduced mean radiant temperature by 3.5–7.7 °C during high-temperature periods, with high-risk areas decreasing by 27–50.4%, and highlighted a significant correlation between aspect ratio and cooling potential[9]. The Burdur case, using the ENVI-met model, showed that thermal comfort in hard-paved areas was 20% lower than in green spaces, proposing adaptive measures like reducing asphalt materials and prioritizing greenery. In thermal vulnerability assessment, Foshan developed a residential subjectivity framework, finding that open dense mid-high-rise

[1]School of Geographical Science and Tourism, Xinjiang Normal University, Urumqi 830017, China. [2]College of Political Science and Law, Xinjiang Normal University, Urumqi 830017, China. [3]College of Foreign Languages, Xinjiang Normal University, Urumqi 830017, China. ✉email: xchenxjnu@xjnu.edu.cn

layouts reduced thermal vulnerability by 4.97% compared to traditional patterns[10]. Zou et al.[11] further integrated local climate zones (LCZs), indicating a positive correlation between building height and the Heat Vulnerability Index, with natural LCZs (e.g., vegetated areas) significantly improving thermal environments. Addressing the heterogeneity of diurnal heat hotspots, Wuhan's research used multi-model machine learning to identify industrial zones as persistent day-night hotspots and mid-high-rise mixed blocks as primary night-time UHI contributors, proposing collaborative optimization of building height and density[12]. Refined building thermal climate zoning in Chongqing's mountainous areas increased zoning coverage from 10.5 to 100%, providing a new paradigm for energy-efficient design in hilly cities[13]. These advancements signal a shift in urban thermal environment research from single-factor analysis to a systematic governance paradigm integrating multi-source data and multi-scale linkages.

UHI refers to a phenomenon where the temperature in urban centers is higher than that in rural or suburban areas[14]. It can be classified into four types: boundary layer UHI (BLUHI), canopy layer UHI (CLUHI), surface UHI (SUHI), and sub-surface UHI (SubUHI)[15–19]. The first two types, BLUHI and CLUHI, pertain to the warming of the urban air temperature (AT) at different vertical scales, which can be directly measured using thermometers. However, the limited and scattered network of meteorological stations can only provide a partial representation of the non-uniform urban/suburban temperature variations[20]. SUHI, on the other hand, refers to the warming of the urban land surface temperature (LST) and is derived from satellite-observed surface temperature data. It is widely recognized that satellite-based remote sensing technology can provide spatially continuous coverage of LST in a time- and cost-effective manner[21]. As a result, in recent years, there has been increasing attention focused on SUHI[22]. UHII is an indicator used to assess the strength of the UHI effect. It is typically characterized by the temperature difference between the urban center and rural/suburban areas[23]. The most commonly used indicators are CLUHII and SUHII[24]. A higher UHII value indicates a greater temperature difference between the urban center and the suburbs/rural areas. Currently, the air pollutants (AP) monitored in China include six major categories: fine particulate matter 2.5 ($PM_{2.5}$), coarse particulate matter 10 (PM_{10}), nitrogen dioxide (NO_2), ozone (O_3), sulfur dioxide (SO_2), and carbon monoxide (CO). In terms of spatiotemporal distribution, areas with high UHII also tend to have higher levels of AP. For example, large cities exhibit higher UHII compared to smaller cities, and economically developed and densely populated urban agglomerations have higher concentrations of AP than other regions[25,26]. Studies have shown that the UHI effect and air pollution often influence each other. The UHI effect causes urban areas to have higher temperatures than surrounding rural areas, and this temperature difference alters the stability of the atmospheric boundary layer. The warm air rises above the city, creating a local low-pressure area that may inhibit the vertical dispersion of pollutants, leading to their accumulation near the ground level in urban areas[27,28]. Aerosols in the air, such as $PM_{2.5}$, PM_{10}, can absorb and scatter solar radiation, reducing the amount of solar energy that reaches the ground and thereby exerting a certain cooling effect during the day. Aerosols also absorb long-wave radiation emitted from the ground and re-radiate heat at night, causing an increase in nighttime temperatures and exacerbating the nighttime UHI effect[29].

There are many factors influencing UHI and AP, such as meteorological conditions, land use/cover, urban morphology (UM), population, and economic development[19,30,31]. With the introduction of themes like "healthy urban planning" and "sustainable development," the influence of UM on UHI has attracted more and more attention. Current research primarily concentrates on the impact of urban organizational form, land use, and street networks within UM on UHI, while there is relatively less research on building characteristics[32–34]. A large number of studies have analyzed the causes of the UHI from two - dimensional (2D) indicators such as landscape metrics, vegetation coverage, impervious surfaces, land types, and population distribution[35]. Quantifying the urban morphology indicators (UMIs) of the above - mentioned urban landscapes has been proven to have an impact on the urban thermal environment[36,37]. However, the characteristics described above are the (2D) features of the city. The three - dimensional (3D) height information of the city plays a crucial role in solar radiation, heat absorption and dissipation, and ventilation. Studies by scholars on Chengdu, China, have shown that the impact of the 3D morphology of the city seems to be more significant than the 2D morphology[38]. A study taking Nanjing as an example shows that increasing building height and reducing building density can create larger shadows under solar radiation, effectively reducing the exposed surfaces of buildings and the city, thus reducing the local AT[39]. However, some studies indicate that the impact of urban 2D morphology indicators is more significant than that of urban 3D morphology[40]. The reasons for this difference may be the different arrangements of urban buildings, economic levels, and climatic factors in the study area, or it may also be due to the differences in temperature types. LST mainly reflects the thermal state of the land surface and cannot accurately reflect the thermal environment at the canopy height. Therefore, it is necessary to compare LST and AT within the same study area.

Many cities around the world have conducted extensive research on AP. Air pollution is not only highly correlated with pollution sources (such as traffic, air conditioning emissions, and industrial pollution), socioeconomic factors, and climatic factors, but is also related to UM[41–43]. In urban areas of the United States, regions with higher building density can capture more air pollution compared to rural or open spaces[44]. Taking Shanghai as an example, 18 UMIs were quantified to study their impact on air pollution. The distance to the main road, the standard deviation of building floors, and the average number of building floors were proven to be the three main UM characteristics affecting the spatial variation of pollutants[45]. Research on the urban center of London shows that UM and vegetation arrangement significantly affect wind speed and direction, exacerbating air pollution in street canyons with different aspect ratios[46]. Research on Seoul, South Korea, indicates that areas with the highest PM concentration are those with high - density traffic and high - rise buildings, as well as areas in close proximity to highways and areas with highly mixed land use[47]. All of the above - mentioned studies demonstrate that UM has a significant impact on AP.

Currently, methods used to study the relationship between UM and climatic variables include linear regression (multiple linear regression, ridge regression, stepwise regression)[21,48], spatial regression models (spatial error model, spatial lag model, geographically weighted regression)[49,50], and machine learning methods (such as XGboost, Random Forest, Artificial Neural Network)[51–53]. Traditional linear regression is simple and fast to operate, with highly interpretable results, but its drawback is that some variables do not conform to linear regression, leading to poor fitting performance[32]. Spatial regression models can reveal the spatial heterogeneity of the impact of urban morphological indicators on climatic variables, but they require indicators with low multicollinearity. Machine learning methods exhibit strong learning capability and flexibility in handling different data formats and complex data, and are widely used without the need to explicitly consider interactions between independent variables; however, they have the disadvantage of overfitting. Although the aforementioned methods each have their advantages, they are primarily suited for studying the relationship between two variables. Due to the complexity of factors influencing UHI, we strive to identify more influencing factors and explore the path relationships between variables, which can be effectively addressed by structural equation modeling. Structural equation modeling, previously utilized mainly in humanities and social science research, is now employed for quantitative research on mediation effects[54,55].

In summary, due to the ease of obtaining LST data, most studies have chosen to investigate SUHI as a variable, neglecting CLUHI. The differences in the distribution of CLUHI and SUHI may result in distinct impacts and mechanisms of UM on CLUHI and SUHI. Secondly, both UMIs and AP have significant effects on UHI, and UMIs also have a notable impact on AP. Therefore, we hypothesize that AP may exacerbate the influence of UMIs on UHI, yet there is currently limited research in this area. We will use a ridge regression model to uncover the differences in the impact of UMIs on the two types of heat island intensities and establish a structural equation model to verify whether AP acts as a mediator between UMIs and UHII. Studying the effects of UMIs on both types of UHII and quantitatively assessing the mediating role of AP will contribute to understanding the complex mechanisms of UMIs' influence. This provides a new perspective on how to optimize UM to maximize urban air or thermal environmental benefits.

Data and methods

Study area

Urumqi (located at 86°37′33″ – 88°58′24″E, 42°45′32″ – 44°08′00″N) is situated in the hinterland of the Eurasian continent and is the inland city farthest from the sea globally. The city has a mid-temperate semi-arid continental climate with an average annual precipitation of 277.6 mm, with the highest precipitation occurring in summer. The northern plain, where people reside, experiences temperatures ranging from 24 to 28 °C in July and − 10–20 °C in January. As of 2024, the administrative division of Urumqi comprises 7 districts and 1 county, covering a total area of 13,800 km^2 with a permanent resident population of 4.0848 million and an urbanization rate reaching 96.56% (https://www.urumqi.gov.cn).

The study area selected is a region within the main urban district, encompassing mixed-use land for commercial services, culture and education, and residential purposes. It includes undeveloped land parcels and urban built-up areas with varying degrees of development intensity, exhibiting diversified urban spatial morphological characteristics (Fig. 1). The spatial extent of the study area stretches north from Pamier street, south to Nanhubei road, east next to Liudaowan road, and west to Nanhudong road, forming a rectangular study unit of approximately 16 km^2. Based on the spatial distribution characteristics of communities and the principle of full coverage, a multi-level road monitoring route with a total length of 22 km was established. Additionally, open spaces within the built-up area that are well-ventilated and less disturbed by the thermal effects of buildings were selected as fixed observation points. These points serve as a spatial comparison reference with the high-density built-up area temperature data obtained through mobile monitoring and satellite image inversion.

Data collection and instruments

Data collection

This study obtained data through two channels: self-monitoring and downloading open-source data. From July 12th to 15th, 2024, we conducted a four-day monitoring period around 13:00–15:30 Beijing time each day. Electric bicycles (Fig. 2(a)) equipped with GPS, HOBO MX2302A, and Aeroqual S500 were used for mobile monitoring to collect data on coordinates, temperature, and air pollutants ($PM_{2.5}$, PM_{10}, NO_2). The instrument parameters are detailed in Table 1. To ensure a relatively uniform spatial distribution of data, the electric bicycles maintained a speed of approximately 10 km/h throughout the monitoring process. Simultaneously with the mobile monitoring, Kestrel 5500 and Kestrel 5400 instruments were installed at fixed stations to obtain temperature data (Fig. 2b).

We downloaded Landsat 9 satellite images from the website of the USGS (https://earthexplorer.usgs.gov/), with a pass time of 12:55:32 Beijing time on July 15, 2023. We used ENVI 5.6.2 software (https://www.l3harrisgeospatial.com/Software-Technology/ENVI) to extract LST from Band 10. The Gaofen-6 satellite images were obtained from the China Centre for Resources Satellite Data and Application (https://www.cresda.com/zgzywxyyzxeng/index.html), with a pass time ranging from 13:23:14 to 13:23:27 Beijing time on August 24, 2023. The panchromatic band has a resolution of 2 m, while the multispectral bands have a resolution of 8 m. Using ENVI 5.6.2 software, we performed radiometric calibration, atmospheric correction, orthorectification, and image fusion on the image. The supervised classification using support vector machine was applied to classify land cover types, primarily to obtain green space area and impervious surface area. The building data used in this study was extracted in ArcGIS 10.8 software with Tianditu Map (https://www.tianditu.gov.cn/) as the base map. The building height data was obtained through field surveys in the study area, assuming a floor height of 3 m for each building, and the product of the number of floors and floor height was used to represent the building height.

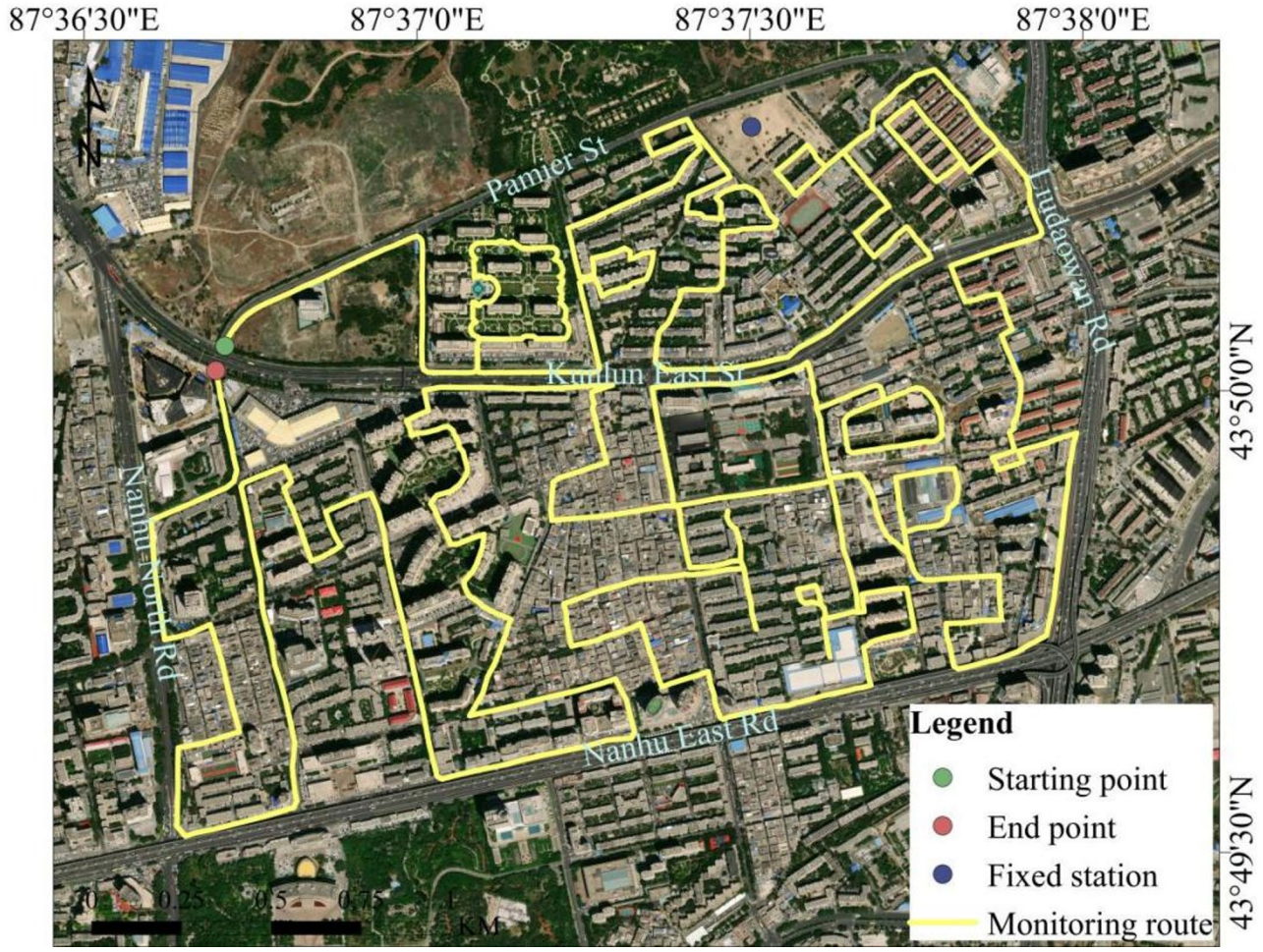

Fig. 1. Study area and monitoring route (Generated in the ArcGIS 10.8 software, URL: http://www.esri.com/).

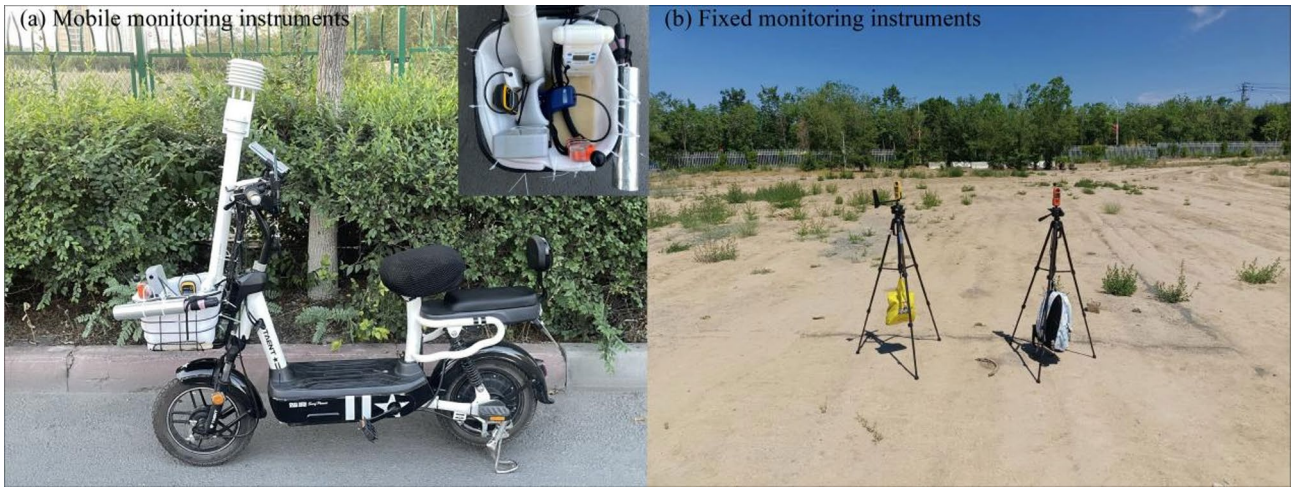

Fig. 2. Measuring instruments.

Urban morphology indicators

We selected eight indicators from both 2D and 3D perspectives[56–58], as shown in Table 2. There are four 2D UMIs, including building density (BD), mean patch shape index (MPSI), impervious surface percent (ISP), and green coverage ratio (GCR), which mainly reflect the density of buildings, the complexity of building shapes, the size of impervious surfaces, and the level of greenery within a buffer zone. There are also four 3D UMIs,

Monitoring scenario	Instrument	Item	Unit	Monitoring interval	Accuracy
Mobile monitoring	GARMIN Etrex 201x	Coordinates	°	5s	3 m
	HOBO MX 2302 A	AT	°C	5s	±0.5 °C
	Aeroqual S500	PM_{10}, $PM_{2.5}$, NO_2	mg/m^3	1 min	<±0.02 mg/m^3
Fixed monitoring	Kestrel 5500, 5400	AT	°C	5s	±0.5 °C

Table 1. Monitoring instrument parameters.

	Indicators	Abbreviation	Definition	Formula
2D	Building density	BD	The total number of buildings per ha in a study area (n/ha)	$BD_i = \frac{NB_i}{A}$ *NB*: the number of building in the *i*th buffer; *A*: the area of a buffer zone
	Mean patch shape index	MPSI	The mean value of building shape complexity	$MPSI_i = \frac{1}{n} \times \sum_{j=1}^{n} \frac{e_j}{mine_i}$ *n*: number of total buildings; e_j: perimeter of the jth building in the buffer zone; $mine_i$: the minimum value of the perimeter of the building in the *i*th buffer zone
	Impervious surface percent	ISP	The ratio of total building footprint area in a buffer to a buffer area (%)	$ISP_i = \frac{M_i}{A}$ M_i: total impervious surface area in *i*th buffer
	Green coverage ratio	GCR	Ratio of green space area to a buffer area (m^2)	$GCR_i = \frac{G_i}{A}$ G_i is the area of green space in the *i*th buffer zone
3D	Mean building area	MBH	The mean height of buildings in a buffer (m)	$MBH_i = \frac{\sum_{j=1}^{n} H_j}{n}$ H_j: the height of the *j*th building
	Standard deviation of building height	BHSD	The extent of buildings change within the study area (m)	$BHSD_i = \sqrt{\frac{\sum_{j=1}^{n} (H_j - MBH)^2}{n}}$
	Floor area ratio	FAR	The ratio of total floor area to a buffer area	$FAR_i = \frac{\sum_{j=1}^{n} (B_j \times F_j)}{A}$ B_j: the floor area of the *j*th building in ith buffer; F_j: the number of floors in the *j*th building in *i*th buffer
	Sky view factor	SVF	The ratio between the radiation received by a planar surface and the entire emispheric radiating environment (%)	$SVF_i = 1 - \sum_{i=1}^{N} sin^2\beta \left(\frac{a_i}{360^\circ}\right)$ $Mean\ SVF_i = \frac{SVF_i}{n}$ *N*: the total number of sectors in the sky hemisphere that are obscured by obstacles; β_i is the angle of maximum building height of each sector; a_i is the azimuthal angle of each sector

Table 2. Description of urban morphology indicators.

including mean building height (MBH), standard deviation of building height (BHSD), floor area ratio (FAR), and sky view factor (SVF), which primarily reflect the average height of all buildings within a buffer zone, the variation in building heights, the development intensity of buildings, and the openness of the sky above the buildings. These indicators, firstly, can comprehensively and accurately characterize the architectural features of UM. Secondly, they are commonly used parameters in urban planning and management, and urban planners and managers need to rely on these indicators to formulate and implement effective mitigation strategies. Thirdly, these indicators possess universality and comparability[56] .

Data processing

In ArcGIS 10.8 software, 500 random points were created along the monitoring route as sample points. Buffers with diameters ranging from 100 m to 500 m were then created centered on these 500 points. Using the summary statistics tool, the average AT and average LST were calculated for each of the five buffer sizes. Subsequently, the corresponding UHII was computed. The difference between the temperature measured at the mobile monitoring points and the temperature measured at the fixed monitoring points was used to represent the CLUHII (Eq. 1), while the difference between the average LST within the mobile point buffers and the average LST within the fixed point buffers was used to represent the SUHII (Eq. 2). If the difference is greater than 0, it indicates that the AT/LST at the mobile monitoring points is higher than that at the fixed points; if the difference is less than 0, it indicates that the AT/LST at the mobile monitoring points is lower than that at the fixed points; if the difference is equal to 0, it indicates that the AT/LST at the mobile monitoring points is the same as that at the fixed points.

$$\mathrm{CLUHII} = \mathrm{AT\_mobile} - \mathrm{AT\_fixed} \tag{1}$$

$$\mathrm{SUHII} = \mathrm{LST\_mobile} - \mathrm{LST\_fixed} \tag{2}$$

In ArcGIS 10.8 software, using tools such as the field calculator and summary statistics, we calculated the mean values of all UMIs and AP for buffers with diameters of 100 m, 200 m, 300 m, 400 m, and 500 m. Ultimately, we obtained the mean values of two types of UHII, as well as the UMIs and AP, for the five buffer sizes. With UMIs and AP as independent variables, and CLUHII and SUHII as dependent variables. Determining the buffer zone diameter is a prerequisite for the study. We conducted a normality test on the UMIs and found that they

did not follow a normal distribution, thus opting for the spearman correlation test. compared to subjectively determining the buffer zone diameter, quantification through the spearman correlation coefficient is more convincing. We calculated the spearman correlation coefficients between UHII and UHIs within buffer zones ranging from 100 to 500 m and compared them. Based on the performance of all indicators, we selected a buffer zone with significant correlations for all indicators as the research unit.

Statistical methods

Ridge regression model

We chose ridge regression to validate the impact of UMIs and AP on UHII. Due to the use of common parameters in the calculation of UMIs, there exists multicollinearity among them. Ridge regression, also known as Tikhonov regularization, is a variant of linear regression. It is suitable for situations where features are highly correlated (i.e., multicollinearity issues), as ordinary linear regression models may become unstable and the model coefficients may become excessively large. By adding a regularization term, Ridge regression constrains the size of the model parameters, making the model more robust. Ridge regression can drive the coefficients of some unimportant features towards zero, thereby serving as a form of feature selection and helping us identify the significant features that have a greater impact on the dependent variable[59,60]. We are implementing ridge regression in SPSS 25 (https://www.ibm.com/) software with the aim of demonstrating the linear relationship between UMIs, AP, and UHII, so that we can establish an structural equation model.

Structural equation model

We utilized structural equation modeling (SEM) to quantify the direct causal relationship between UMIs and UHII, as well as the indirect relationship mediated by AP[61]. SEM simulates multivariate relationships using two or more structural equations and presents intuitive graphics to depict complex relational networks. Therefore, SEM can assess the complex relationships among multiple variables, surpassing traditional multivariate linear regression methods. SEM has the advantage of explaining the partial contributions of related variables and distinguishing between direct and indirect effects, meaning it can differentiate various pathways through which one entity influences another and then estimate and compare the strengths of these different pathways[62]. In this study, we developed a SEM (Fig. 3) to analyze the relationships among UMIs, AP and UHII using Amos 26. The inter-factor path coefficients were systematically examined. 'a' represents the path coefficient for the impact of UM on AT. 'b' represents the path coefficient for the impact of AT on UHII. 'c' represents the total effect, which is the path coefficient for the impact of UM on UHII without the mediator variable. 'c' represents the direct effect, which is the path coefficient for the impact of UM on UHII with the mediator variable involved. 'a*b' represents the mediation effect value, and the mediation effect proportion is calculated by dividing the mediation effect value by the total effect. Through constructing the initial model and multiple revisions, the final model passed the tests and assessments of indices such as the chi-square to degrees of freedom ratio (X^2/DF < 3), Goodness-of-Fit Index (GFI > 0.90), Comparative Fit Index (CFI > 0.90), Root Mean Square Error of Approximation (RMSEA < 0.08), and significance ($P > 0.05$)[63,64]. The flowchart of this study is shown in Fig. 4.

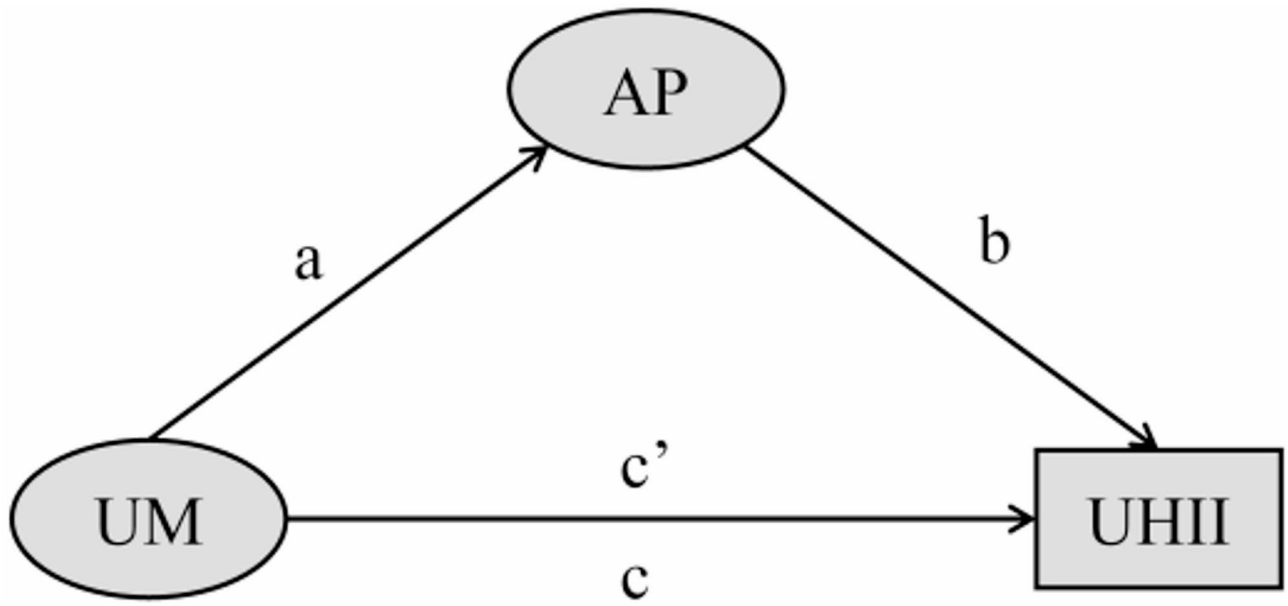

Fig. 3. Mediating effect model.

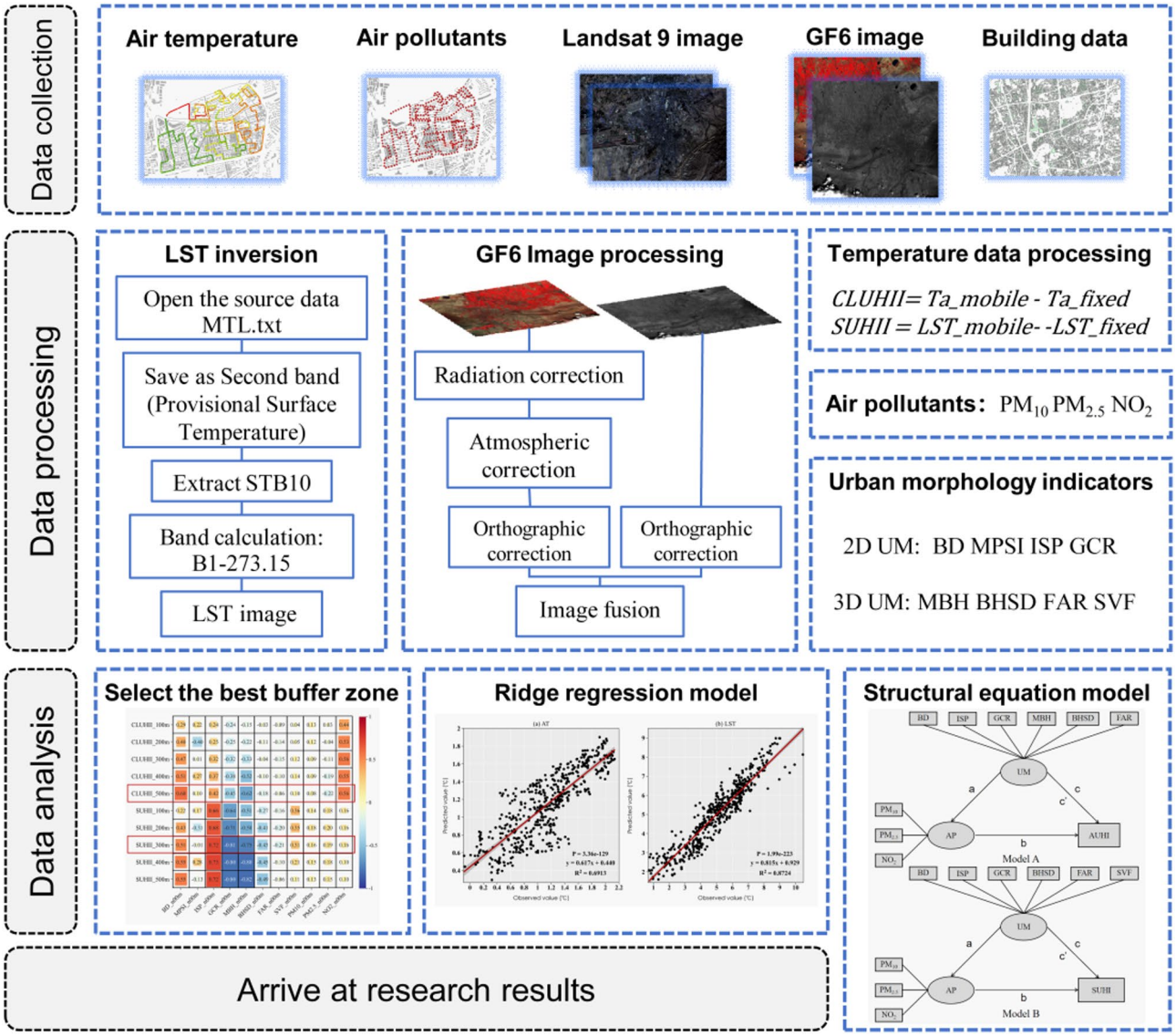

Fig. 4. Study framework.

Results

Determination of optimal buffer zone

Fig. 5 presents the spearman correlation coefficients of UHII, UMIs, and AP across different buffer zones. The results indicate that the correlation between MPSI and CLUHII is unstable. The correlations of FAR and SVF with CLUHII exhibit a trend of increasing first and then decreasing. The correlations of BD, ISP, GCR, MBH, BHSD, $PM_{2.5}$, and NO_2 with CLUHII all intensify as the buffer diameter increases, reaching their peak at a buffer diameter of 500 m. The correlations of BD, MBH, and BHSD with SUHII increase with the expansion of the buffer diameter. The correlation between MPSI and SUHII is unstable. The correlations of ISP, GCR, PM_{10}, and $PM_{2.5}$ with SUHII decrease as the buffer diameter increases, peaking at diameters ranging from 200 to 400 m. The correlations of SVF and NO_2 with SUHII gradually diminish as the buffer diameter increases. Overall, the correlations between SUHII and various indicators are relatively strong at a buffer diameter of 300 m. Based on this comprehensive analysis, we will investigate the impact of UMIs and AP on CLUHII within a buffer zone of 500 m in diameter and analyze their influence on SUHII within a buffer zone of 300 m in diameter.

Spatial distribution of AT, LST and AP

Fig. 6 shows the average values of AT and LST in various regions, and their distributions exhibit spatial heterogeneity. The lowest AT is 33.62 °C, while the highest reaches 37.12 °C. Higher Ta values are observed in blocks 9, 14, 17, 27, 28, and 48, whereas lower values are found in blocks 1, 2, 3, 19, 22, and 31. The highest LST is 54.15 °C, and the lowest is 44.29 °C. Higher LST values are concentrated in blocks 40, 59, and 60, while lower values are seen in blocks 0, 45, 46, and 49. There are both similarities and differences in the high and low values of Ta and LST within the same region. For example, in blocks 6, 8, 29, and 30, both Ta and LST show high or low

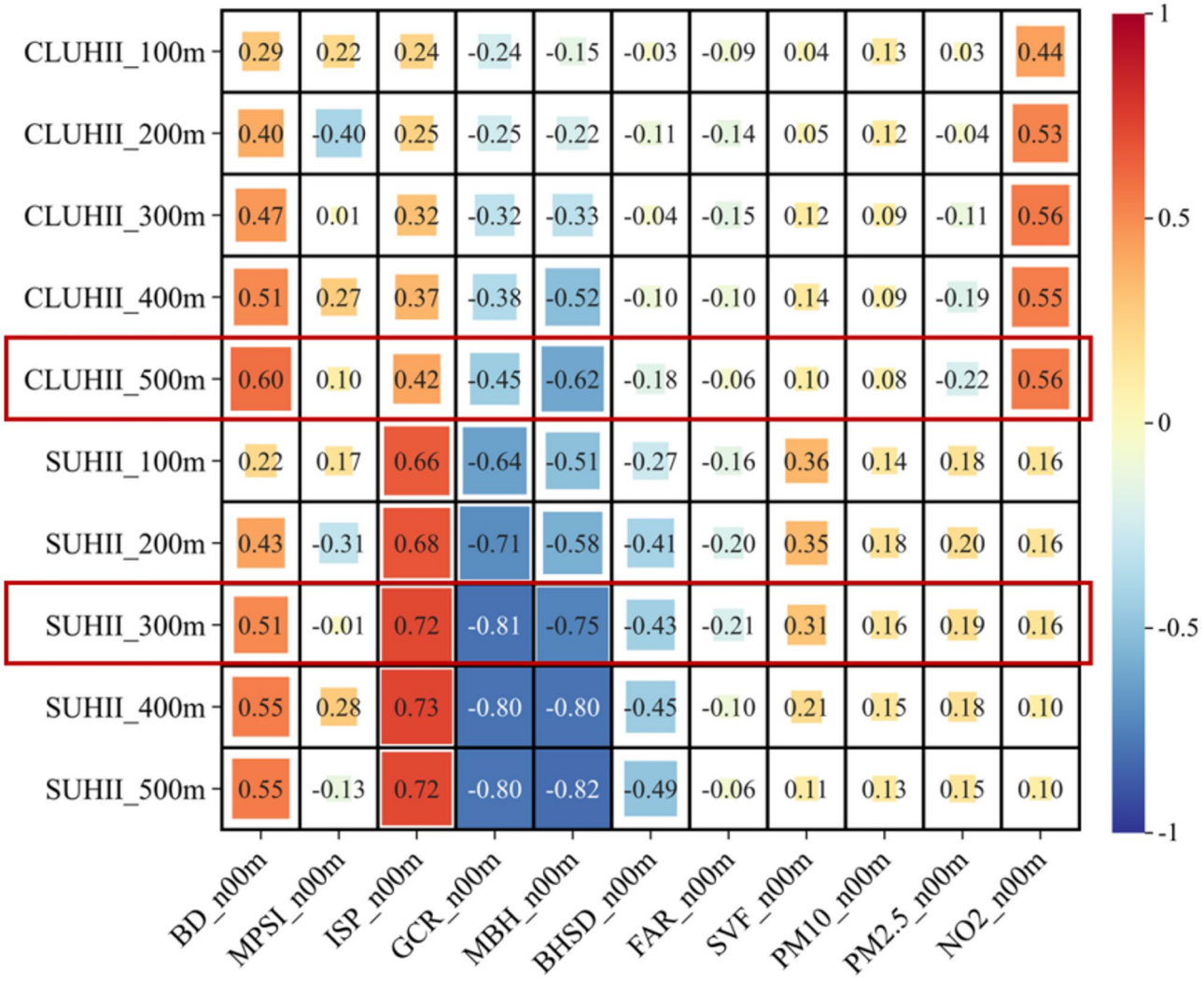

Fig. 5. Spearman correlation coefficient between urban morphology indicators, air pollutants and CLUHII and SUHII.

Fig. 6. The spatial distribution of average AT (**a**) and LST (**b**) of blocks (Generated in the ArcGIS 10.8 software, URL: http://www.esri.com/).

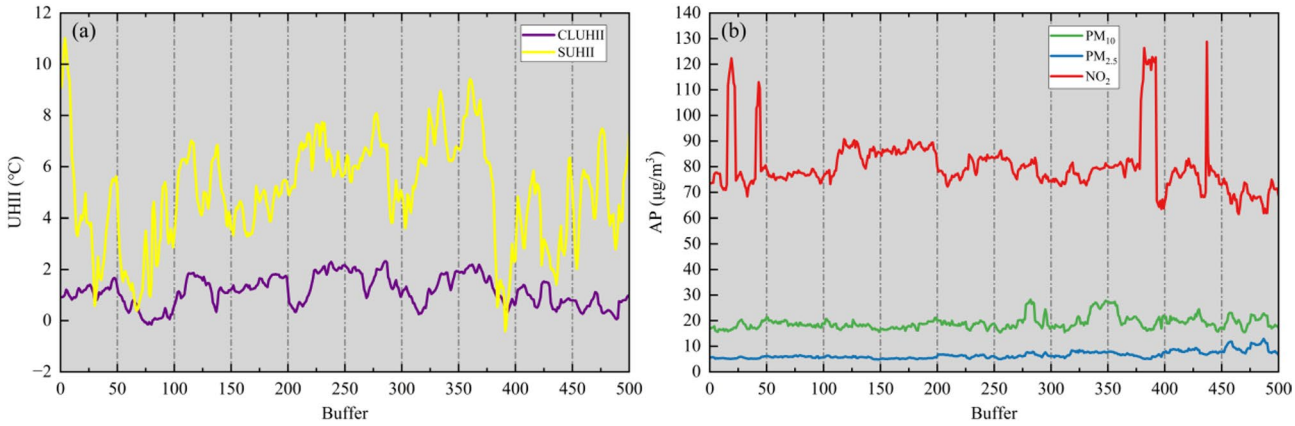

Fig. 7. UHII (**a**) and air pollutants (**b**) distribution in buffer zones.

	CLUHII				SUHII			
	Non-standardized coefficient		standardized coefficient		Non-standardized coefficient		standardized coefficient	
	B	Std.err.	Beta	P	B	Std.err.	Beta	P
Constant	35.394	0.431	–	0.000***	45.833	0.541	–	0.000***
BD	11.23	2.802	0.122	0.000***	83.891	7.483	0.186	0.000***
MPSI	0	0	0.034	0.183	0	0	− 0.103	0.000***
ISP	0.894	0.097	0.221	0.000***	1.461	0.142	0.151	0.000***
GCR	− 0.867	0.122	− 0.18	0.000***	− 4.981	0.16	− 0.44	0.000***
MBH	− 0.024	0.003	− 0.281	0.000***	− 0.027	0.003	− 0.15	0.000***
BHSD	0.022	0.003	0.256	0.000***	− 0.024	0.004	− 0.117	0.000***
FAR	0.013	0.038	0.01	0.743	− 0.123	0.05	− 0.044	0.015**
SVF	− 1.332	0.401	− 0.099	0.001***	7.446	0.523	0.237	0.000***
PM_{10}	0.012	0.008	0.043	0.141	0.036	0.009	0.065	0.000***
$PM_{2.5}$	0.061	0.014	0.129	0.000***	− 0.132	0.019	− 0.117	0.000***
NO_2	0.005	0.002	0.074	0.007***	0.004	0.002	0.027	0.076*
K	0.139				0.143			
R^2	0.605				0.869			
R^2_adj	0.596				0.866			
F	68.013 (0.000***)				291.511 (0.000***)			

Table 3. Ridge regression result. ***, ** and * represent the significance levels of 1%, 5% and 10% respectively.

values simultaneously. However, in blocks 7, 40, 41, and 48, the high and low values of Ta and LST are opposite. We found that this is related to the BD, building height (BH), and GCR. In the districts with high building density and low GCR, both AT and LST are relatively high, such as blocks 8, 27, 28, 29, and 30. In the districts with high BD, high BH, and high GCR, AT is often lower while LST is higher, such as blocks 0, 1, 2, 3, 40, and 41. This may be because green spaces can reduce the AT, but the LST of green spaces has a relatively small effect on reducing the high LST caused by high BD.

Fig. 7 shows the average concentrations of CLUHII, SUHII, and three types of AP within the buffer zones along the route. CLUHII fluctuates between 0 and 3 °C, with a relatively small range of variation. SUHII fluctuates between − 1 and 12 °C, with a large range of variation, which may be due to the large temperature differences among various types of surfaces. The average concentrations of PM_{10} and $PM_{2.5}$ are relatively low, while the concentration of NO_2 is higher than that of the previous two pollutants and has a greater variation range, which may be related to the traffic conditions and BD of each buffer zone.

Effects of UM and AP on UHII

Table 3 presents the regression results with UHII_AT and SUHII as dependent variables, respectively, and UMIs and AP as independent variables. All models have passed the F-test ($P = 0.000^{***}$), indicating that the models are statistically significant overall. UMIs and AP can explain 59.6% of the spatial variability in CLUHII. Based on the regression coefficients of each indicator, the degree of influence of UMIs on CLUHII is: BD > SVF > ISP > GCR > MBH > BHSD. The indicators that positively impact CLUHII are BD, ISP, BHSD, and

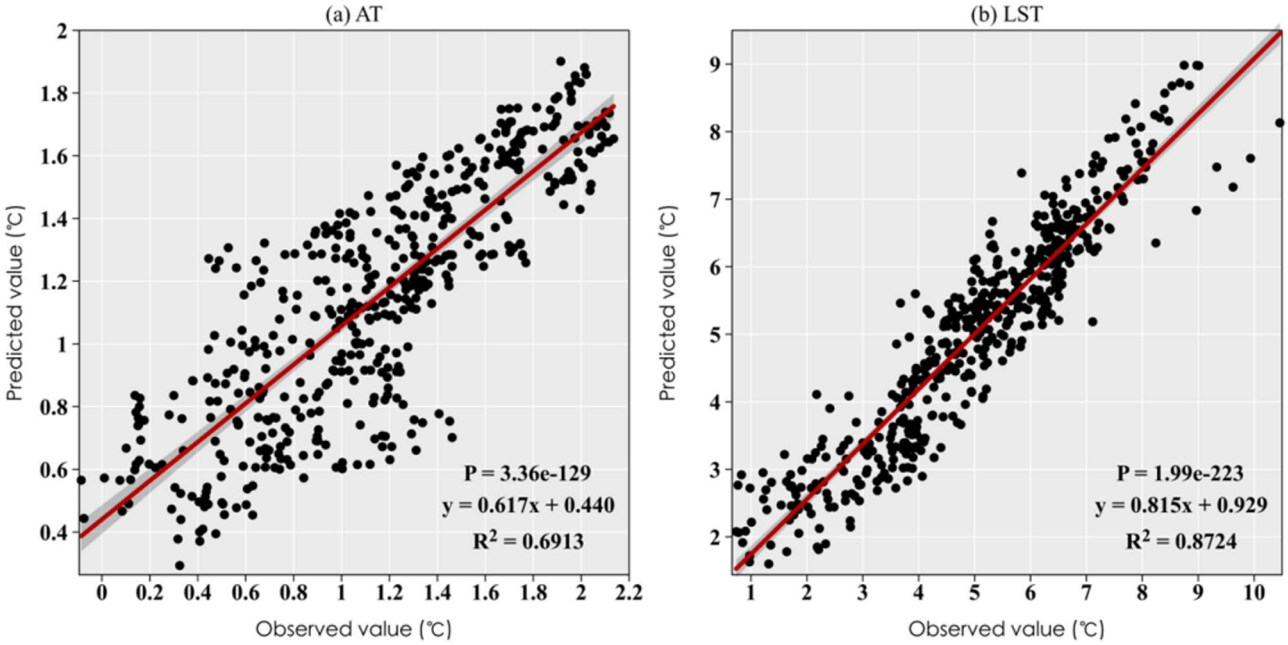

Fig. 8. Linear regression between the predicted value and the actual value of the ridge regression model.

	X^2/DF	GFI	CFI	RMSE
Model A	1.15	0.99	1.00	0.02
Model B	1.10	0.99	1.00	0.01

Table 4. Test results of model parameters.

FAR (although the impact of FAR is not significant). The indicators that negatively impact CLUHII are GCR, MBH, SVF, and MPSI. Among AP, all have a positive impact on CLUHII, with $PM_{2.5}$ having the greatest impact, followed by NO_2 and then PM_{10}.

UMIs and AP can explain 86.6% of the spatial variability in SUHII. According to the regression coefficients of each indicator, the degree of influence of UMIs on SUHII is: BD > SVF > GCR > ISP > FAR > MBH > BHSD. The indicators that positively impact SUHII are BD, ISP, and SVF. The indicators that negatively impact SUHII are GCR, MBH, BHSD, and FAR (the impact of MPSI is not significant). Among air pollutants (AP), all have a positive impact on SUHII, with $PM_{2.5}$ having the greatest impact, followed by PM_{10} and then NO_2.

When comparing the two models, the fit between UMIs, AP, and SUHII is better, meaning that UMIs and AP can explain more of the spatial variability in SUHII and have a stronger predictive power for SUHII (Fig. 8). Among the UMIs, BD and ISP both positively impact both CLUHII and SUHII, while GCR, MBH, and BHSD all negatively impact both. The impact of MPSI is insignificant for both. The impacts of FAR and SVF on CLUHII and SUHII are opposite.

Model fitting and parameter test

Based on the results of the ridge regression model, although most UMIs and AP have significant impacts on both CLUHII and SUHII, the pathways of their influences need further exploration. Based on empirical assumptions, it is hypothesized that AP plays a mediating role in the impact of UMIs on UHII. By removing the insignificant paths calculated and re-computing the model, the obtained parameters were compared with standard values (Table 4). Both Model A and Model B have X^2/DF values less than 3, GFI values greater than 0.90, CFI values greater than 0.90, and RMSE values less than 0.08, indicating a good fit of the model results. This suggests that AP indeed plays a mediating role in the impact of UMIs on UHII. The model diagram is shown in Fig. 9.

Mediating effect of air pollutants

Table 5 presents the total effect, mediation effect value, indirect effect, and proportion of mediation effect for the significant paths. PM_{10}, $PM_{2.5}$, and NO_2 each play a mediating role in the impact of different UMIs on UHII. Specifically, PM_{10} partially mediates the impact of BD on CLUHII, with a mediation effect proportion of 4.214%, indicating that 4.214% of the increase in UHII caused by BD is due to the accumulation of PM_{10}. $PM_{2.5}$ partially mediates the impacts of BD, GCR, BHSD, and FAR on CLUHII, and fully mediates the impact of ISP on CLUHII. NO_2 partially mediates the impacts of BD, BHSD, and FAR on CLUHII, with mediation effect proportions of 7.253%, 10.081%, and 10.171%, respectively.

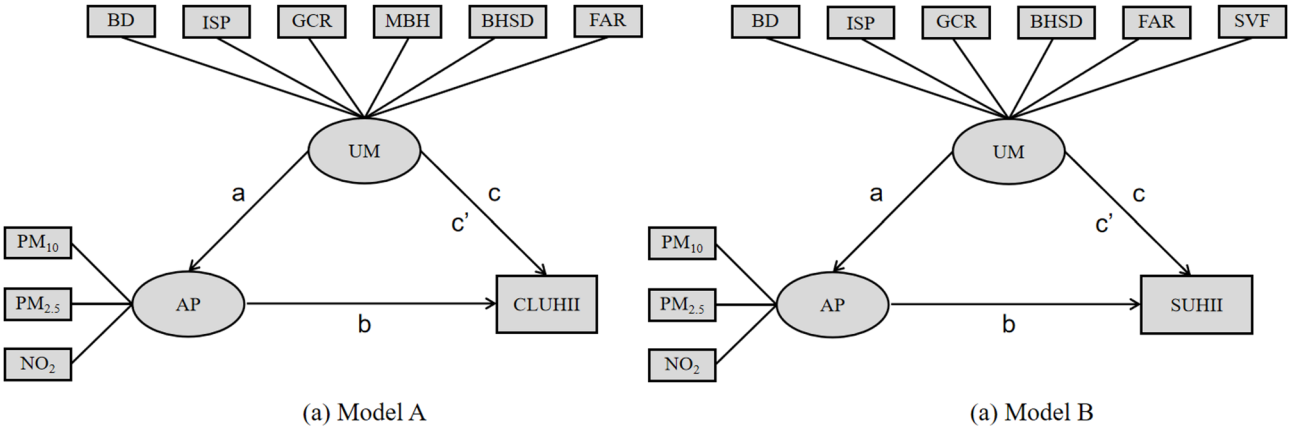

Fig. 9. SEM model, (**a**) CLUHII is the dependent variable, (**b**) SUHII is the dependent variable.

Item	c	a*b	c'	Proportion of mediating effect (%)	Conclusion
BD = > PM_{10} = > CLUHII	57.136	2.407	45.382	4.214	Partial mediation
ISP = > PM_{10} = > CLUHII	− 0.058	0.314	− 0.063	100	Complete mediation
SVF = > PM_{10} = > CLUHII	− 0.623	0.206	− 0.735	100	Complete mediation
BD = > $PM_{2.5}$ = > CLUHII	57.136	5.203	45.382	9.106	Partial mediation
ISP = > $PM_{2.5}$ = > CLUHII	− 0.058	− 0.393	− 0.063	100	Complete mediation
GCR = > $PM_{2.5}$ = > CLUHII	− 1.265	− 0.297	− 1.298	23.491	Partial mediation
BHSD = > $PM_{2.5}$ = > CLUHII	0.051	0.005	0.044	10.815	Partial mediation
FAR = > $PM_{2.5}$ = > CLUHII	− 0.789	− 0.094	− 0.662	11.912	Partial mediation
BD = > NO_2 = > CLUHII	57.136	4.144	45.382	7.253	Partial mediation
BHSD = > NO_2 = > CLUHII	0.051	0.005	0.044	10.081	Partial mediation
FAR = > NO_2 = > CLUHII	− 0.789	− 0.08	− 0.662	10.171	Partial mediation
BD = > PM_{10} = > SUHII	135.187	4.593	112.209	3.40	Partial mediation
BHSD = > PM_{10} = > SUHII	− 0.033	− 0.006	− 0.034	17.04	Partial mediation
FAR = > PM_{10} = > SUHII	− 0.275	0.049	− 0.066	100	Complete mediation
BD = > $PM_{2.5}$ = > SUHII	135.187	15.735	112.209	11.64	Partial mediation
ISP = > $PM_{2.5}$ = > SUHII	− 4.946	− 0.845	− 4.449	17.08	Partial mediation
GCR = > $PM_{2.5}$ = > SUHII	− 13.126	− 0.978	− 12.467	7.45	Partial mediation
MBH = > $PM_{2.5}$ = > SUHII	0.002	0.011	− 0.011	100	Complete mediation
FAR = > $PM_{2.5}$ = > SUHII	− 0.275	− 0.198	− 0.066	100	Complete mediation
BD = > NO_2 = > SUHII	135.187	2.65	112.209	1.96	Partial mediation
MBH = > NO_2 = > SUHII	0.002	0.002	− 0.011	100	Complete mediation
FAR = > NO_2 = > SUHII	− 0.275	− 0.06	− 0.066	100	Complete mediation

Table 5. The proportion of mediating effect results.

PM_{10} partially mediates the impacts of BD and BHSD on SUHII, with mediation effect proportions of 3.4% and 17.04%, respectively, and fully mediates the impact of FAR on SUHII. $PM_{2.5}$ partially mediates the impacts of BD, ISP, and GCR on SUHII, with mediation effect proportions of 11.64%, 17.08%, and 7.45%, respectively, and fully mediates the impact of MBH_FAR on SUHII. NO_2 partially mediates the impact of BD on SUHII, with a mediation effect proportion of 1.96%, and fully mediates the impacts of MBH and FAR on SUHII.

Discussion

The influence mechanism of UMIs on CLUHII and SUHII

The spatial heterogeneity of CLUHII and SUHII is caused by the interaction of various factors in urban areas, such as building clusters, underlying surfaces, vegetation, and human activities. Since CLUHII reflects the temperature difference in AT, while SUHII reflects the temperature difference in LST, the mechanisms through which UMIs affect them are different.

In this study, BD has a positive impact on both CLUHI and SUHII. An increase in BD may affect the building's wind environment, hindering air circulation and thus increasing AT. For SUHII, a higher BD implies a greater number of buildings and a larger proportion of impervious surfaces. The materials of the buildings absorb solar radiation, resulting in higher LST on the building surfaces[65]. MPSI has an insignificant impact on

both CLUHII and SUHII in this study. ISP has a significant positive effect on both CLUHII and SUHII. The reason is that impervious surfaces, often made of cement or asphalt, cannot cool down by evaporating water like soil or vegetation. The AT is absorbed by the impervious surface and continuously releases heat, exacerbating the rise in AT. For SUHII, impervious surfaces absorb a large amount of solar radiation and convert it into heat energy, leading to an increase in LST. GCR has a significant negative effect on both CLUHII and SUHII. During transpiration, GCR consumes a large amount of heat, thereby reducing the ambient AT. For SUHII, the transpiration of green spaces can lower their own surface temperature. Additionally, tree canopies and shade reduce solar radiation and LST[66].MBH has a negative effect on both CLUHII and SUHII. Taller buildings create larger building shadows, which have a cooling effect on both AT and LST[67]. The impact of BHSD on CLUHII and SUHII is opposite. BHSD has a significant positive effect on CLUHII. A higher BHSD indicates greater variation in building heights within the buffer zone. Large variations in building heights (such as staggered building clusters) can disrupt wind flow, hinder natural ventilation, lead to the retention of hot air, and result in localized temperature increases, thus elevating CLUHII. In contrast, BHSD has a negative effect on SUHII. Staggered buildings cast shadows at different times of the day, reducing the time the surface is directly exposed to sunlight and thus lowering LST.

Our research results show that the impacts of FAR and SVF on CLUHII and SUHII are opposite, which is closely related to the urban building layout. FAR has a positive impact on CLUHII and a significant negative impact on SUHII. A high FAR means that there are massive and densely distributed buildings in the city. A large number of building entities occupy space. These building materials (such as concrete, bricks, etc.) absorb a large amount of solar radiation during the day and become a continuous heat source, directly increasing the temperature in the canopy layer. Therefore, it shows a positive impact on CLUHII. The communities in the study area are mostly commercial - residential mixed land. The human activities and equipment operation in commercial buildings generate a large amount of heat, and the dense buildings make it difficult for the heat to dissipate, promoting the increase of CLUHII[68]. However, at the urban surface, although the buildings are dense, the tall buildings can block the direct sunlight on the ground to a certain extent, reducing the absorption of solar radiation by the surface. Moreover, the shaded areas of the buildings are relatively cool, resulting in a decrease in SUHII. Thus, it shows a negative impact on SUHII[53]. SVF has a negative impact on CLUHII and a significant positive impact on SUHII. A high SVF indicates that there are more open spaces in the city. At the canopy level, there is less obstruction of the sky by buildings, and the air circulation in the canopy is relatively smooth, which is not conducive to the accumulation of heat island intensity. Therefore, it shows a negative impact on CLUHII. In the canopy, the transpiration of plants consumes heat, and the open space is conducive to the dissipation of heat to the sky, which is beneficial for reducing CLUHII[69]. At the urban surface, the open space allows more solar radiation to directly reach the ground. Most of the surfaces in the study area are cement buildings and asphalt pavements. These surfaces absorb a large amount of heat and then the temperature rises, showing a positive impact on SUHII[20].

AP form a complex intermediary network between UM and UHII by regulating the radiation budget, heat exchange processes, and photochemical reactions[70]. UMIs leads to the accumulation of $PM_{2.5}$ and PM_{10} by obstructing air circulation. Aerosol particles scatter short-wave solar radiation, reducing the solar radiation received by the surface, which in turn lowers the LST during the day and alters the surface albedo[71]. Secondly, pollutants (such as particulate matter) settle on building surfaces or vegetation, decreasing the surface albedo and increasing the absorption of solar radiation, which will increase the UHII[72].Although we have explained the mechanisms influencing UHII in terms of UM and air pollution, the real situation is much more complex. The increase in UHII is the result of the combined effects of multiple indicators.

The synergistic effect of UMIs and influence mechanism

By calculating the spearman correlation coefficients among the UMIs metrics, it has been found that there are interaction effects among the UMI metrics (Fig. 10). When the UMIs have an impact on the UHII, different metrics do not act in isolation. Instead, they jointly shape the heat island effect through complex interactions[12]. For instance, BD, GCR, and ISP exhibit spatial competition-type interaction effects, and they have a synergistic enhancement effect on UHII. An increase in BD directly leads to a decrease in the GCR (as it occupies green space) and an increase in the ISP (due to the increase in building bases and hard surfaces), forming a "double-driven heat island effect". The reduction of green space weakens the transpiration cooling of vegetation and the reflection of solar radiation. The increase in ISP enhances the absorption of short-wave radiation by the surface (such as the high heat absorption of asphalt and concrete) and the retention of long-wave radiation, causing the surface and the atmosphere to warm up, thus increasing both the CLUHII and the SUHII. FAR, MBH, BHSD, and SVF show 3D spatial form interaction effects. A high FAR is often accompanied by an increase in MBH and a decrease in SVF (with dense and tall buildings blocking the sky), giving rise to the "canyon effect". After the solar radiation absorbed by the building surface is converted into long-wave radiation, it is difficult to dissipate into the upper air due to the low SVF, resulting in heat accumulation near the ground. At the same time, in areas with a high FAR, there is a dense population and a large number of facilities, releasing a great deal of anthropogenic heat, which, when combined with the surface heat storage, exacerbates the SUHII. A high BHSD (such as a mixed layout of high and low buildings) may alleviate the heat island effect by forming "ventilation corridors" (promoting air flow in areas of low-rise buildings), while a low BHSD (high-density building clusters with uniform heights) may suppress air convection and enhance heat retention. Exploring the interaction effects among these indicators can provide a reliable reference for urban planning and drive the transformation from single-metric control to systematic morphological optimization.

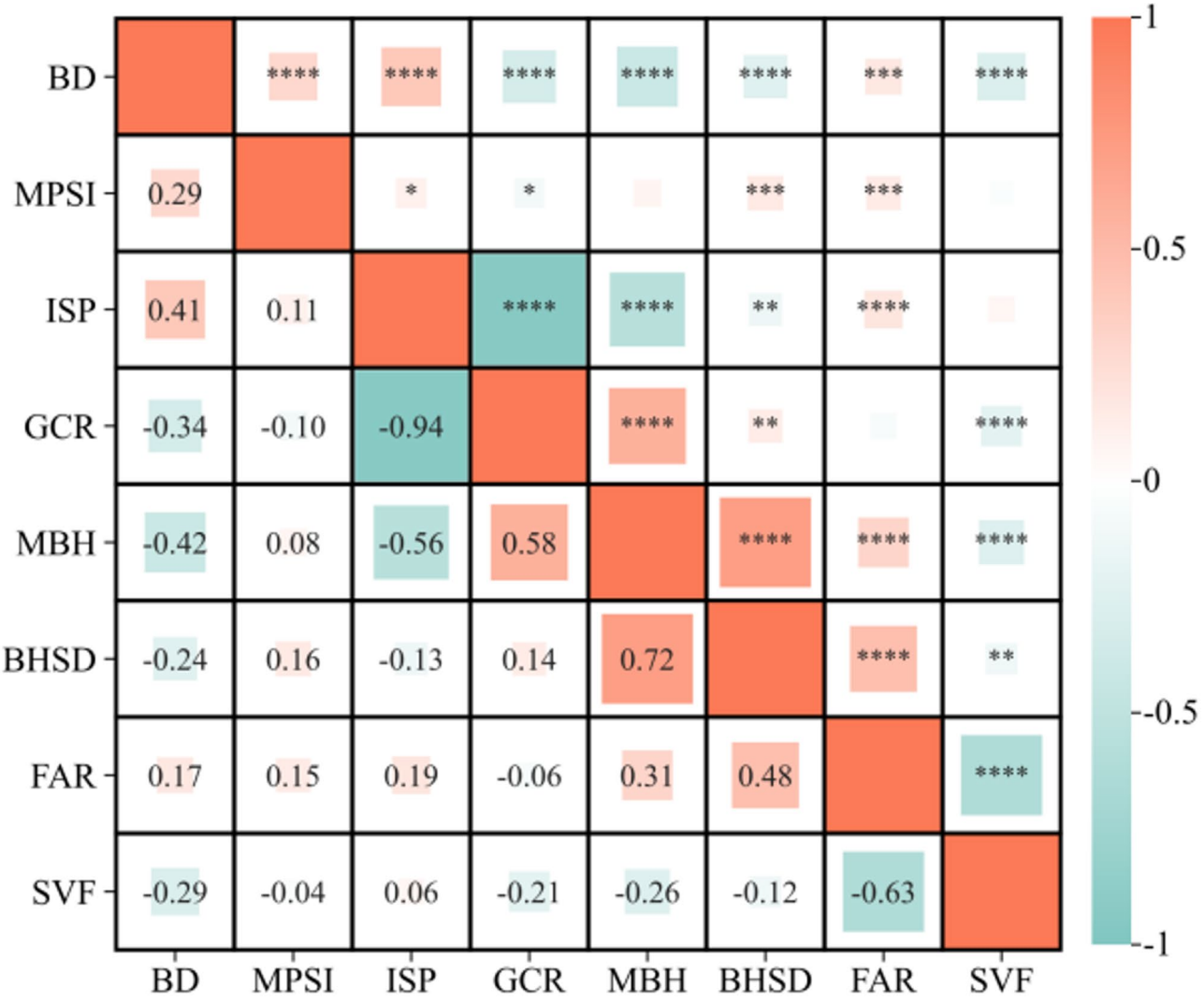

Fig. 10. The spearman correlation coefficient among urban morphological indicators.

Implications of urban planning and management

Understanding the relationship among UM, AP, and the UHII is of great significance for improving the UHI effect and urban planning management[73–75]. Studies have shown that AP play a significant mediating role in the impact of UMIs on the CLUHII and the SUHII. UMIs can affect the diffusion and accumulation of AP. The change in the concentration of AP, in turn, affects the energy balance and heat exchange process of the city, ultimately acting on the UHII. We can mitigate the UHII through two approaches. One is to optimize UM to prevent the accumulation of air pollutants. For the already developed downtown areas, it is unrealistic to reduce building density and the proportion of impervious surfaces. We can increase parks, green spaces, and street trees to provide shade and lower the temperature[76]. Promoting green roofs can reduce the heat absorption of building rooftops[77]. Encouraging residents to plant vegetation on balconies and in courtyards can increase the local GCR. Using light - colored, high - reflectivity building materials and paints can increase the reflection of solar radiation and reduce heat absorption. Painting rooftops and walls white or in light colors can effectively lower the LST of buildings, further reducing indoor temperatures and alleviating the UHI effect[78–80]. The second is to mitigate UHII by reducing air pollutant emissions. We recommend giving priority to the development of high - capacity public transportation systems such as subways, light rail, and bus rapid transit, encouraging residents to commute in a green way, reducing the use of private cars, and decreasing the heat generated by vehicle emissions and traffic congestion.

Limitations and prospects

Firstly, this study only focused on the impact of UMIs on CLUHII and SUHII during midday in summer. Urumqi has a long and cold winter. During the heating period, the combustion of coal releases a large amount of pollutants such as $PM_{2.5}$, PM_{10}, and SO_2, resulting in poor air quality. The presence of a large number of pollutants may enhance the absorption of long - wave radiation from the ground by the atmosphere, and the proportion of the mediating effect of AP may increase. At night in summer, without direct sunlight, the heat stored in buildings

begins to be slowly released. Although the traffic flow at night decreases, and the heat and exhaust emissions from motor vehicles are significantly reduced, and the heat and pollution generated by humans also decrease, the heat and pollutants accumulated during the day may accumulate in buildings due to poor ventilation, and the UHII may be stronger compared to that during the day. Therefore, it is necessary to conduct a comparative study of summer and winter, as well as day and night in the future. Secondly, this study was conducted at a micro-scale and only one sample area was selected. With a limited number of urban meteorological stations, it is challenging to represent AT and AP in small areas. By adopting a mobile monitoring approach, we were able to obtain higher-resolution AT and AP data. However, obtaining high-resolution AT and AP data at a larger scale remains a challenge, and this is one of our future research endeavors.

Summary and conclusions

In this work, we visualized the collected AT and LST data and observed spatial heterogeneity between them. By comparing the Spearman correlation coefficients between UMIs, AP, and the two types of UHII, we identified the optimal research units. The best research units for studying the relationships between UMIs, AP, CLUHII, and SUHII were found to be buffer zones with diameters of 500 m and 300 m, respectively. Subsequently, we established ridge regression models with the two types of UHII as dependent variables and UMIs and AP as independent variables. These models revealed the differential impacts of UMIs on CLUHII and SUHII and explored the mechanisms through which UMIs influence these two types of UHII. Compared to CLUHII, UMIs and AP could explain more of the spatial variability in SUHII. MPSI had an insignificant impact on both, while BHSD, FAR, and SVF had opposite effects on them. Finally, we constructed a structural equation model to verify that all three types of AP had significant mediating effects between some UMIs and UHII.

Currently, global cities are generally facing unprecedented urbanization processes, aggravated UHI effects, and air pollution problems. This study breaks through the limitations of previous research in understanding the mechanism by which UMIs affect UHI, systematically analyzing the action paths and differences of UMIs on different types of UHII. Secondly, it quantitatively evaluates the mediating effect of AP in the association between UMIs and UHII, filling the gap in the field of quantitative analysis. The research findings not only deepen the understanding of the relationship among UM, the UHI effect, and air pollution but also provide a new theoretical basis and practical direction for optimizing the planning and design of UMIs in global cities and jointly alleviating the UHI effect and air pollution. It also supplements crucial empirical support for subsequent research on urban sustainable development and policy formulation.

Data availability

All data generated or analyzed during this study are included in this published article.

Received: 21 September 2024; Accepted: 15 May 2025
Published online: 26 May 2025

References

1. Zhang, M., Tan, S., Zhang, C. & Chen, E. Machine learning in modelling the urban thermal field variance index and assessing the impacts of urban land expansion on seasonal thermal environment. *Sci. Total Environ.* **106**, 105345. https://doi.org/10.1016/j.scs.2024.105345 (2024).
2. Kim, S. W. & Brown, R. D. Urban heat Island (UHI) intensity and magnitude estimations: A systematic literature review. *Sci. Total Environ.* **779**, 146389. https://doi.org/10.1016/j.scitotenv.2021.146389 (2021).
3. Hu, C. et al. Tracking the impact of the land cover change on the spatial-temporal distribution of the thermal comfort: insights from the Qinhuai river basin, China. *Sci. Total Environ.* **116**, 105916. https://doi.org/10.1016/j.scs.2024.105916 (2024).
4. Luo, X. et al. Analysis on spatial-temporal features of taxis' emissions from big data informed travel patterns: a case of Shanghai, China. *J. Clean. Prod.* **142**, 926–935. https://doi.org/10.1016/j.jclepro.2016.05.161 (2017).
5. Yu, W. et al. Shared insights for heat health risk adaptation in metropolitan areas of developing countries. *iScience* **27**, 109728. https://doi.org/10.1016/j.isci.2024.109728 (2024).
6. Banerjee, S. et al. Analysing impacts of urban morphological variables and density on outdoor microclimate for tropical cities: A review and a framework proposal for future research directions. *Build. Environ.* **225**, 109646. https://doi.org/10.1016/j.buildenv.2022.109646 (2022).
7. Zhang, J., Li, Z. & Hu, D. Effects of urban morphology on thermal comfort at the micro-scale. *Sci. Total Environ.* **86**, 104150. https://doi.org/10.1016/j.scs.2022.104150 (2022).
8. Wu, W., Li, L. & Li, C. Seasonal variation in the effects of urban environmental factors on land surface temperature in a winter City. *J. Clean. Prod.* **299**, 126897. https://doi.org/10.1016/j.jclepro.2021.126897 (2021).
9. Guo, F., Guo, R., Zhang, H., Dong, J. & Zhao, J. A canopy shading-based approach to heat exposure risk mitigation in small squares. *Urban Clim.* **49**, 101495. https://doi.org/10.1016/j.uclim.2023.101495 (2023).
10. Zhang, M. et al. Impact of urban surfaces on microclimatic conditions and thermal comfort in Burdur, Türkiye. *Atmosphere* **15** (1375). https://doi.org/10.3390/atmos15111375 (2024).
11. Zou, Q., Yang, J., Zhang, Y., Bai, Y. & Wang, J. Variation in community heat vulnerability for Shenyang City under local climate zone perspective. *Build. Environ.* **267**, 112242. https://doi.org/10.1016/j.buildenv.2024.112242 (2025).
12. Liu, H., Li, M., Zhan, Q., Ma, Z. & He, B. J. Homogeneity and heterogeneity of diurnal and nocturnal hotspots and the implications for synergetic mitigation in heat-resilient urban planning. *Comput. Environ. Urban.* **117**, 102241. https://doi.org/10.1016/j.compenvurbsys.2024.102241 (2025).
13. Zhang, T. et al. Refined Building thermal climate zoning scheme in regions with mountainous terrain for accurate Building energy-saving potential Estimation. *Energ. Build.* **313**, 114228. https://doi.org/10.1016/j.enbuild.2024.114228 (2024).
14. Voogt, J. A. & Oke, T. R. Thermal remote sensing of urban climates. *Remote Sens. Environ.* **86**, 370–384. https://doi.org/10.1016/S0034-4257(03)00079-8 (2003).
15. Sekertekin, A. & Zadbagher, E. Simulation of future land surface temperature distribution and evaluating surface urban heat Island based on impervious surface area. *Ecol. Indic.* **122**, 107230. https://doi.org/10.1016/j.ecolind.2020.107230 (2021).
16. Pichierri, M., Bonafoni, S. & Biondi, R. Satellite air temperature Estimation for monitoring the canopy layer heat Island of Milan. *Remote Sens. Environ.* **127**, 130–138. https://doi.org/10.1016/j.rse.2012.08.025 (2012).

17. Yuan, F. & Bauer, M. E. Comparison of impervious surface area and normalized difference vegetation index as indicators of surface urban heat Island effects in Landsat imagery. *Remote Sens. Environ.* **106**, 375–386. https://doi.org/10.1016/j.rse.2006.09.003 (2007).
18. Qian, Y. et al. Urbanization impact on regional climate and extreme weather: current understanding, uncertainties, and future research directions. *Adv. Atmos. Sci.* **39**, 819–860. https://doi.org/10.1007/s00376-021-1371-9 (2022).
19. Li, Y. et al. A systematic review of studies involving canopy layer urban heat Island: monitoring and associated factors. *Ecol. Indic.* **158**, 111424. https://doi.org/10.1016/j.ecolind.2023.111424 (2024).
20. Kim, J. et al. The effect of extremely low Sky view factor on land surface temperatures in urban residential areas. *Sci. Total Environ.* **80**, 103799. https://doi.org/10.1016/j.scs.2022.103799 (2022).
21. Tong, S. et al. Study on correlation between air temperature and urban morphology parameters in built environment in Northern China. *Build. Environ.* **127**, 239–249. https://doi.org/10.1016/j.buildenv.2017.11.013 (2018).
22. Shi, T., Liu, L., Wen, X. & Qi, P. Research progress on the synergies between heat waves and canopy urban heat Island and their driving factors. **12**. https://doi.org/10.3389/fenvs.2024.1363837 (2024).
23. Yang, Q. et al. A global urban heat Island intensity dataset: generation, comparison, and analysis. *Remote Sens. Environ.* **312**, 114343. https://doi.org/10.1016/j.rse.2024.114343 (2024).
24. Yao, R. et al. Long-term trends of surface and canopy layer urban heat Island intensity in 272 cities in the Mainland of China. *Sci. Total Environ.* **772**, 145607. https://doi.org/10.1016/j.scitotenv.2021.145607 (2021).
25. Li, X., Zhou, Y., Asrar, G. R., Imhoff, M. & Li, X. The surface urban heat Island response to urban expansion: A panel analysis for the conterminous united States. *Sci. Total Environ.* **605–606**, 426–435. https://doi.org/10.1016/j.scitotenv.2017.06.229 (2017).
26. Wu, J., Zheng, H., Zhe, F., Xie, W. & Song, J. Study on the relationship between urbanization and fine particulate matter (PM2.5) concentration and its implication in China. *J. Clean. Prod.* **182**, 872–882. https://doi.org/10.1016/j.jclepro.2018.02.060 (2018).
27. Cichowicz, R. & Bochenek, A. D. Assessing the effects of urban heat Islands and air pollution on human quality of life. *Anthropocene* **46**, 100433. https://doi.org/10.1016/j.ancene.2024.100433 (2024).
28. Ulpiani, G. On the linkage between urban heat Island and urban pollution Island: Three-decade literature review towards a conceptual framework. *Sci. Total Environ.* **751**, 141727. https://doi.org/10.1016/j.scitotenv.2020.141727 (2021).
29. Zender-Świercz, E., Galiszewska, B., Telejko, M. & Starzomska, M. The effect of temperature and humidity of air on the concentration of particulate matter - PM2.5 and PM10. *Atmos. Res.* **312**, 107733. https://doi.org/10.1016/j.atmosres.2024.107733 (2024).
30. wang, A., Zhang, M., Chen, E., Zhang, C. & Han, Y. Impact of seasonal global land surface temperature (LST) change on gross primary production (GPP) in the early 21st century. *Sci. Total Environ.* **110**, 105572. https://doi.org/10.1016/j.scs.2024.105572 (2024).
31. Deilami, K., Kamruzzaman, M. & Liu, Y. Urban heat Island effect: A systematic review of spatio-temporal factors, data, methods, and mitigation measures. *Int. J. Appl. Earth Obs Geoinf.* **67**, 30–42. https://doi.org/10.1016/j.jag.2017.12.009 (2018).
32. Zhang, P., Ghosh, D. & Park, S. Spatial measures and methods in sustainable urban morphology: A systematic review. *Landsc. Urban Plan.* **237**, 104776. https://doi.org/10.1016/j.landurbplan.2023.104776 (2023).
33. Elmarakby, E. & Elkadi, H. Impact of urban morphology on urban heat Island in Manchester's transit-oriented development. *J. Clean. Prod.* **434**, 140009. https://doi.org/10.1016/j.jclepro.2023.140009 (2024).
34. Jiang, Z., Cheng, H., Zhang, P. & Kang, T. Influence of urban morphological parameters on the distribution and diffusion of air pollutants: A case study in China. *J. Environ. Sci.* **105**, 163–172. https://doi.org/10.1016/j.jes.2020.12.035 (2021).
35. Shen, Y. et al. Stereoscopic urban morphology metrics enhance the nonlinear scale heterogeneity modeling of UHI with explainable AI. *Urban Clim.* **56**, 102006. https://doi.org/10.1016/j.uclim.2024.102006 (2024).
36. Chen, J. et al. Seasonally disparate responses of surface thermal environment to 2D/3D urban morphology. *Build. Environ.* **214**, 108928. https://doi.org/10.1016/j.buildenv.2022.108928 (2022).
37. Han, D. et al. Understanding seasonal contributions of urban morphology to thermal environment based on boosted regression tree approach. *Build. Environ.* **226**, 109770. https://doi.org/10.1016/j.buildenv.2022.109770 (2022).
38. Luo, P. et al. How 2D and 3D built environments impact urban surface temperature under extreme heat: A study in Chengdu, China. *Build. Environ.* **231**, 110035. https://doi.org/10.1016/j.buildenv.2023.110035 (2023).
39. Chen, Y. et al. Relationship between urban Spatial form and seasonal land surface temperature under different grid scales. *Sci. Total Environ.* **89**, 104374. https://doi.org/10.1016/j.scs.2022.104374 (2023).
40. Berger, C. et al. Spatio-temporal analysis of the relationship between 2D/3D urban site characteristics and land surface temperature. *Remote Sens. Environ.* **193**, 225–243. https://doi.org/10.1016/j.rse.2017.02.020 (2017).
41. Sekmoudi, I. et al. Systematic review of air pollution in Morocco: status, impacts, and future directions. *Adv. Sustainable Syst.* **8**, 2400006. https://doi.org/10.1002/adsu.202400006 (2024).
42. Liu, Y., Wu, J. & Yu, D. Disentangling the complex effects of socioeconomic, Climatic, and urban form factors on air pollution: A case study of China. *Sustainability* **10**, 776. https://doi.org/10.3390/su10030776 (2018).
43. Zhang, J. et al. Comparing multiple machine learning models to investigate the relationship between urban morphology and PM2.5 based on mobile monitoring. *Build. Environ.* **248**, 111032. https://doi.org/10.1016/j.buildenv.2023.111032 (2024).
44. Ngo, N. S., Zou, Z., Yang, Y. & Wei, E. The impact of urban form on the relationship between vehicle Miles traveled and air pollution. *Transp. Res. Interdiscip Perspect.* **28**, 101288. https://doi.org/10.1016/j.trip.2024.101288 (2024).
45. Li, C., Wang, Z., Li, B., Peng, Z. R. & Fu, Q. Investigating the relationship between air pollution variation and urban form. *Build. Environ.* **147**, 559–568. https://doi.org/10.1016/j.buildenv.2018.06.038 (2019).
46. Borna, M., Turci, G., Marchetti, M. & Schiano-Phan, R. Evaluating the influence of urban blocks on air pollution concentration levels: the case study of golden lane estate in London. *Sustainability* **16**, 696. https://doi.org/10.3390/su16020696 (2024).
47. Ahn, H., Lee, J. & Hong, A. Urban form and air pollution: clustering patterns of urban form factors related to particulate matter in Seoul, Korea. *Sci. Total Environ.* **81**, 103859. https://doi.org/10.1016/j.scs.2022.103859 (2022).
48. Wen, D. et al. A comparative study of the effects of urban morphology on land surface temperature in Chengdu and Chongqing, China. *Sci. Rep.* **14**, 25130. https://doi.org/10.1038/s41598-024-77036-y (2024).
49. Yin, C., Yuan, M., Lu, Y., Huang, Y. & Liu, Y. Effects of urban form on the urban heat Island effect based on Spatial regression model. *Sci. Total Environ.* **634**, 696–704. https://doi.org/10.1016/j.scitotenv.2018.03.350 (2018).
50. Fan, J., Chen, X., Xie, S. & Zhang, Y. Study on the response of the summer land surface temperature to urban morphology in Urumqi, China. *Sustainability* **15** (2023).
51. Yuan, B., Zhou, L., Hu, F. & Wei, C. Effects of 2D/3D urban morphology on land surface temperature: contribution, response, and interaction. *Urban Clim.* **53**, 101791. https://doi.org/10.1016/j.uclim.2023.101791 (2024).
52. Tian, L. et al. Examining the non-linear relationship between urban form and air temperature at street level: A case of Hong Kong. *Build. Environ.* **264**, 111884. https://doi.org/10.1016/j.buildenv.2024.111884 (2024).
53. Wu, Y., Che, Y., Liao, W. & Liu, X. The impact of urban morphology on land surface temperature across urban-rural gradients in the Pearl river delta, China. *Build. Environ.* **267**, 112215. https://doi.org/10.1016/j.buildenv.2024.112215 (2025).
54. Liang, Z. et al. The mediating effect of air pollution in the impacts of urban form on nighttime urban heat Island intensity. *Sci. Total Environ.* **74**, 102985. https://doi.org/10.1016/j.scs.2021.102985 (2021).
55. Fan, J., Chen, X., Xie, S. & Du, K. Mediating effect of air pollutants on urban morphology and air temperature. *Atmos. Pollut Res.* **16**, 102426. https://doi.org/10.1016/j.apr.2025.102426 (2025).
56. Zhou, R. et al. Quantifying the relationship between 2D/3D Building patterns and land surface temperature: study on the metropolitan Shanghai. *Remote Sens.* **14**, 4098. https://doi.org/10.3390/rs14164098 (2022).

57. Zhang, J., Cui, P. & Song, H. Impact of urban morphology on outdoor air temperature and microclimate optimization strategy base on Pareto optimality in Northeast China. *Build. Environ.* **180**, 107035. https://doi.org/10.1016/j.buildenv.2020.107035 (2020).
58. Xu, H., Chen, H., Zhou, X., Wu, Y. & Liu, Y. Research on the relationship between urban morphology and air temperature based on mobile measurement: A case study in Wuhan, China. *Urban Clim.* **34**, 100671. https://doi.org/10.1016/j.uclim.2020.100671 (2020).
59. Hoerl, A. E. & Kennard, R. W. J. T. Ridge regression: biased Estimation for nonorthogonal problems. *Technometrics* **42**, 80–86. https://doi.org/10.1080/00401706.1970.10488634 (2000).
60. Lan, Y. & Zhan, Q. How do urban Buildings impact summer air temperature? The effects of Building configurations in space and time. *Build. Environ.* **125**, 88–98. https://doi.org/10.1016/j.buildenv.2017.08.046 (2017).
61. Grace, J. B. *Structural Equation Modeling and Natural Systems*. *Cambridge University Press*, (2006). https://doi.org/10.1017/CBO9780511617799.
62. Eisenhauer, N., Bowker, M. A., Grace, J. B. & Powell, J. R. From patterns to causal understanding: structural equation modeling (SEM) in soil ecology. *Pedobiologia* **58**, 65–72. https://doi.org/10.1016/j.pedobi.2015.03.002 (2015).
63. Trivedi, P. et al. Microbial regulation of the soil carbon cycle: evidence from gene–enzyme relationships. *ISME J.* **10**, 2593–2604. https://doi.org/10.1038/ismej.2016.65 (2016).
64. Zhu, L. et al. Effects of hydrological environment on litter carbon input into the surface soil organic carbon pool in the Dongting lake floodplain. *CATENA* **208**, 105761. https://doi.org/10.1016/j.catena.2021.105761 (2022).
65. Song, J. et al. Effects of Building density on land surface temperature in China: Spatial patterns and determinants. *Landsc. Urban Plann.* **198**, 103794. https://doi.org/10.1016/j.landurbplan.2020.103794 (2020).
66. El-Hattab, M. Monitoring and assessment of urban heat Islands over the Southern region of Cairo Governorate, Egypt. *Egypt. J. Remote Sens.* **21**, 311–323. https://doi.org/10.1016/j.ejrs.2017.08.008 (2018).
67. Chen, Y., Wu, J., Yu, K. & Wang, D. Evaluating the impact of the Building density and height on the block surface temperature. *Build. Environ.* **168**, 106493. https://doi.org/10.1016/j.buildenv.2019.106493 (2020).
68. Lau, T. K. & Lin, T. P. Investigating the relationship between air temperature and the intensity of urban development using on-site measurement, satellite imagery and machine learning. *Sci. Total Environ.* **100**, 104982. https://doi.org/10.1016/j.scs.2023.104982 (2024).
69. Chen, L. et al. Sky view factor analysis of street canyons and its implications for daytime intra-urban air temperature differentials in high-rise, high-density urban areas of Hong Kong: a GIS-based simulation approach. *Int. J. Climtol.* **32**, 121–136. https://doi.org/10.1002/joc.2243 (2012).
70. Wang, Y., Guo, Z. & Han, J. The relationship between urban heat Island and air pollutants and them with influencing factors in the Yangtze river delta, China. *Ecol. Indic.* **129**, 107976. https://doi.org/10.1016/j.ecolind.2021.107976 (2021).
71. Huang, C. et al. Effect of urban morphology on air pollution distribution in high-density urban blocks based on mobile monitoring and machine learning. *Build. Environ.* **219**, 109173. https://doi.org/10.1016/j.buildenv.2022.109173 (2022).
72. Yao, J. et al. Dry deposition effect of urban green spaces on ambient particulate matter pollution in China. *Sci. Total Environ.* **900**, 165830. https://doi.org/10.1016/j.scitotenv.2023.165830 (2023).
73. Sun, F., Liu, M., Wang, Y., Wang, H. & Che, Y. The effects of 3D architectural patterns on the urban surface temperature at a neighborhood scale: relative contributions and marginal effects. *J. Clean. Prod.* **258**, 120706. https://doi.org/10.1016/j.jclepro.2020.120706 (2020).
74. Chun, B. & Guldmann, J. M. Spatial statistical analysis and simulation of the urban heat Island in high-density central cities. *Landsc. Urban Plan.* **125**, 76–88. https://doi.org/10.1016/j.landurbplan.2014.01.016 (2014).
75. Wang, Y. & Akbari, H. Analysis of urban heat Island phenomenon and mitigation solutions evaluation for Montreal. *Sci. Total Environ.* **26**, 438–446. https://doi.org/10.1016/j.scs.2016.04.015 (2016).
76. Cai, X., Yang, J., Zhang, Y., Xiao, X. & Xia, J. Cooling Island effect in urban parks from the perspective of internal park landscape. *Hum. Soc. Sci. Commun.* **10**, 674. https://doi.org/10.1057/s41599-023-02209-5 (2023).
77. Zhao, S., Dong, J., Guo, F., Zhang, H. & Zhu, P. Optimization of green space in high-density built-up areas based on cooling simulations: A case study in Xi'an, China. *Urban Clim.* **58**, 102225. https://doi.org/10.1016/j.uclim.2024.102225 (2024).
78. Yue, W., Liu, X., Zhou, Y. & Liu, Y. Impacts of urban configuration on urban heat Island: an empirical study in China mega-cities. *Sci. Total Environ.* **671**, 1036–1046. https://doi.org/10.1016/j.scitotenv.2019.03.421 (2019).
79. Kikegawa, Y., Genchi, Y., Kondo, H. & Hanaki, K. Impacts of city-block-scale countermeasures against urban heat-island phenomena upon a building's energy-consumption for air-conditioning. *Appl. Energy*. **83**, 649–668. https://doi.org/10.1016/j.apenergy.2005.06.001 (2006).
80. Aflaki, A. et al. Urban heat Island mitigation strategies: A state-of-the-art review on Kuala Lumpur, Singapore and Hong Kong. *Cities* **62**, 131–145. https://doi.org/10.1016/j.cities.2016.09.003 (2017).

Acknowledgements

I would like to thank my classmates: Siqi Xie, Kaili Du, Mingyue Xi, Yujie Liu, and Yunyao Feng for helping me complete the experiment monitoring together.

Author contributions

J.F. was primarily responsible for writing the manuscript. X.C. provided the topic selection, experimental materials, and funding support, and also optimized the paper. W.Z. offered suggestions for the manuscript. M.Z. participated in data organization and processing. X.Y. polished the language and funding support. All the authors reviewed the manuscript.

Funding

The research was sponsored by the Natural Science Foundation of Xinjiang Uygur Autonomous Region (No. 2022D01A212), the National Natural Science Foundation of China (No. 41861033) and the Humanities and Social Sciences Research Projects of the Ministry of Education of China (No.22YJA740032).

Declarations

Competing interests

The authors declare no competing interests.

Additional information

Correspondence and requests for materials should be addressed to X.C.